Environmental Science & Technology

Article

pubs.acs.org/est

Sodium Rivals Silver as Single-Atom Active Centers for Catalyzing Abatement of Formaldehyde

Yaxin Chen,[†,§] Jiayi Gao,[†,§] Zhiwei Huang,[†] Meijuan Zhou,[†] Junxiao Chen,[†] Chao Li,[†] Zhen Ma,[†] Jianmin Chen,[†] and Xingfu Tang*[,†,‡]

[†]Institute of Atmospheric Sciences, Shanghai Key Laboratory of Atmospheric Particle Pollution & Prevention (LAP[3]), Department of Environmental Science & Engineering, Fudan University, Shanghai 200433, China

[‡]Jiangsu Collaborative Innovation Center of Atmospheric Environment & Equipment Technology (CICAEET), Nanjing University of Information Science & Technology, Nanjing 210044, China

Supporting Information

ABSTRACT: The development of efficient alkali-based catalysts for the abatement of formaldehyde (HCHO), a ubiquitous air pollutant, is economically desirable. Here we comparatively study the catalytic performance of two single-atom catalysts, Na_1/HMO and Ag_1/HMO (HMO = Hollandite manganese oxide), in the complete oxidation of HCHO at low temperatures, in which the products are only CO_2 and H_2O. These catalysts are synthesized by anchoring single sodium ions or silver atoms on HMO(001) surfaces. Synchrotron X-ray diffraction patterns with structural refinement together with transmission electron microscopy images demonstrate that single sodium ions on the HMO(001) surfaces of Na_1/HMO have the same local structures as silver atoms of Ag_1/HMO. Catalytic tests reveal that Na_1/HMO has higher catalytic activity in low-temperature oxidation of HCHO than Ag_1/HMO. X-ray photoelectron spectra and soft X-ray absorption spectra show that the surface lattice oxygen of Na_1/HMO has a higher electronic density than that of Ag_1/HMO, which is responsible for its higher catalytic efficiency in the oxidation of HCHO. This work could assist the rational design of cheap alkali metal catalysts for controlling the emissions of volatile organic compounds such as HCHO.

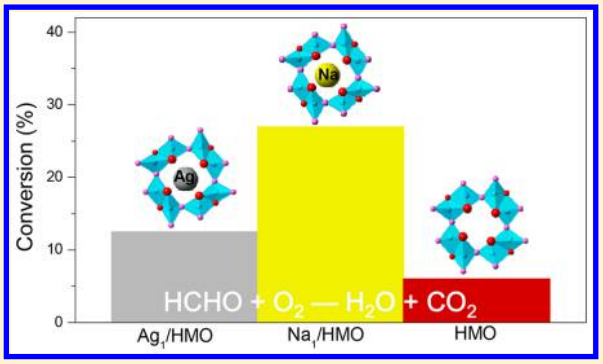

INTRODUCTION

Formaldehyde (HCHO), emitted from building and furnishing materials, is one of the main indoor pollutants that is harmful to human health.[1] Furthermore, it can also take part in some important atmospheric processes[2,3] and contributes to photochemical pollution and catalytic ozone destruction. Therefore, it is crucial to control the HCHO emission. Heterogeneous catalytic oxidation of HCHO over transition metal oxides or supported metal catalysts is one of the most promising technologies, because efficient catalysts can convert HCHO into CO_2 and H_2O.[4−6] Often, supported noble metal catalysts show much higher catalytic activity in HCHO oxidation than transition metal oxides, and hence attract great attention,[6−11] but they are very expensive. To reduce the cost of noble metal catalysts, two strategies are often used: to improve the dispersion degree of noble metals, and to strengthen the metal−support interactions. Highly dispersed Pt catalysts with a low Pt loading showed excellent catalytic performance in the complete oxidation of HCHO at low temperatures.[7,9] Surface-confined atomic silver catalysts with strong metal−support interactions enhanced catalytic efficiency for HCHO removal.[11,12]

An appealing alternative is to use alkali metals to enhance the performance of noble metal catalysts in catalytic oxidation. For instance, Zhang et al.[7,8] improved the catalytic activity of Pt/TiO_2 or Pd/TiO_2 by adding sodium, and they attributed the enhancement of catalytic activity to the increase of adsorbed OH groups active for HCHO oxidation. Similar results were reported by Nie et al.[13] Bai et al.[14] used potassium to enhance the performance of Ag/Co_3O_4 for HCHO abatement. These authors believed that alkali ions only serve as promoters. Likewise, a single Pt atom surrounded by six potassium atoms to form a PtK_6 octahedron with a Pt core could facilitate the activation of oxygen species in the water−gas shift reaction.[15] Although all surface atoms are K atoms, the authors still believed that the core Pt atoms are active sites.

The promotion effect of alkali metals has been reported in many catalytic reactions,[16−20] especially in the synthesis of ammonia,[18] and the Fischer−Tropsch reactions.[19] Occasionally, alkali ions can also promote oxide catalysts.[16,17] Although noble metals often show higher catalytic activity than alkali metals in many reactions, alkali (or alkaline earth) metals atomically dispersed on the supports' surfaces can be very active in some

Received: January 26, 2017
Revised: May 15, 2017
Accepted: May 24, 2017
Published: May 24, 2017

DOI: 10.1021/acs.est.7b00499
Environ. Sci. Technol. 2017, 51, 7084−7090

catalytic oxidation.[21,22] For example, isolated Ca^{2+} sites in hydroxyapatite tunnels were reported to be highly active for HCHO oxidation.[21] Single-site K^+ catalysts were found to be active for HCHO abatement because the K^+ ions with the hybridized *d-sp* orbitals showed significant activation ability toward both gaseous oxygen and lattice oxygen.[22] Therefore, it is vital to differentiate the function of alkalis from that of noble metals under identical conditions.

In this work, we comparatively study the single-atom sodium and silver catalysts by anchoring single sodium or silver on the (001) surfaces of Hollandite manganese oxide (HMO), to shed light on the functions of alkali metals (Scheme 1). Synchrotron

Scheme 1. Structural Models of Catalytically Active Centers of HMO, Ag_1/HMO, and Na_1/HMO[a]

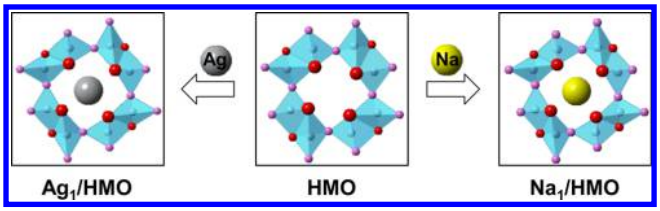

[a]Grey, red, pink, and yellow balls represent Ag, O with sp^3 hybridization, O with sp^2 hybridization, and Na atoms, respectively. Blue octahedron is MnO_6.

X-ray diffraction (SXRD) patterns with a structural refinement and transmission electron microscopy (TEM) images with energy dispersive X-ray spectroscopy (EDX) mapping are used to determine the location of the sodium or silver atoms. Catalytic performance of the single-atom catalysts in HCHO oxidation is studied. The electronic states and the metal–support interactions are revealed by X-ray absorption spectra and X-ray photoelectron spectra (XPS). This work assists the rational design of cheap alkali metal catalysts for controlling the emissions of volatile organic compounds (VOCs) such as HCHO.

EXPERIMENTAL SECTION

Catalyst Preparation. The synthesis of samples was reported in our recent work.[11,23] Briefly, HMO was prepared by a refluxing route and the resulting powders were calcined in air at 400 °C for 4 h (see details in the Supporting Information, SI).[23] Ag_{NP}/HMO was first prepared by using the redox reactions,[11] dried at 80 °C for 24 h, and calcined at 400 °C in air for 4 h to get Ag_1/HMO (see details in the SI). The atomic ratio of Ag/Mn is ~0.15 for Ag_1/HMO, as determined by using X-ray fluorescence spectrometer (XRF) on a Bruker-AXS S4 Explorer. NaCl/HMO was prepared by impregnating HMO powders with an aqueous solution of NaCl, followed by being dried at 80 °C for 12 h. Na_1/HMO was obtained after annealing NaCl/HMO at 400 °C for 12 h and then washing the powder by deionized H_2O at room temperature. The atomic ratio of Na/Mn is ~0.18 for Na_1/HMO, as determined by using XRF.

Catalytic Evaluation. The complete oxidation of HCHO was performed in a fixed-bed quartz reactor (i.d. = 8 mm) under atmospheric pressure. For each run, the reaction temperature began at room temperature, and was increased to the specified temperature at a rate of 1 °C min^{-1}. After holding the temperature for 1 h, the steady state would usually be reached, and the temperature would be held for another half an hour for data collecting. A fresh catalyst (50 mg, 40–60 mesh) was charged for each run. HCHO was generated by passing N_2 over paraformaldehyde (96%, Acros) in an incubator kept at 45 °C. The HCHO gas was mixed with flowing O_2 to get a feed gas (100 mL min^{-1}) containing 140 ppm of HCHO, 10.0 vol % O_2, and balance N_2. The products of the reaction were analyzed by an online Agilent 7890A GC equipped with a TCD detector. The HCHO conversion was calculated from a carbon balance, i.e., 1 mol HCHO forms 1 mol CO_2. The HCHO conversion (X_{HCHO}) was calculated from the CO_2 content as follows:

$$X_{HCHO}\ (\%) = \frac{[CO_2]_{out}}{[HCHO]_{in}} \times 100\%$$

where $[CO_2]_{out}$ and $[HCHO]_{in}$ in the formula are the CO_2 concentration in the products and the HCHO concentration of the flow gas, respectively.

For kinetics analysis, the X_{HCHO} is kept below 20%. Turnover frequency (TOF) is defined as the number of HCHO molecules converted per active site per second (see details in the SI).

Catalyst Characterizations. SXRD patterns were recorded at BL14B of the Shanghai Synchrotron Radiation Facility (SSRF) at a wavelength of 0.6883 Å. Rietveld refinements of the diffraction data were performed with the FULLPROF software package on the basis of the space group *I*4/*m*. TEM, high-resolution TEM (HRTEM), and scanning TEM (STEM) with EDX mapping were conducted on a JEM 2100F transmission electron microscope. XPS were collected using the Kratos Axis Ultra-DLD system with a charge neutralizer and a 150 W Al (Monochromatized) X-ray gun (1486.6 eV) with an energy resolution of ~0.15 eV. The spectrometer was equipped with a delay-line detector. Spectra were acquired at normal emission with a passing energy of 40 eV. XPS data were referenced to the C 1*s* peak at the binding energy (BE) of 284.6 eV. Data analysis and processing were undertaken using the XPSPeak4.1 software with the Shirley type background. The soft X-ray absorption spectra at the O *K*-edge were measured in a total electron yield (TEY) mode at the 4B7B of the Beijing Synchrotron Radiation Facility (BSRF).

Density Function Theory (DFT) Calculations. DFT calculations were performed using the Vienna ab initio simulation package (VASP).[24,25] The electronic structure of all the configurations was calculated using the generalized gradient approximation (GGA)[26] method with the Perdew–Burke–Ernzerhof (PBE)[27] exchange-correlation function. All the structures were calculated with the plane-waves energy cutoff of 450 eV. The lattice parameter of NaCl crystal with the cubic space group *Fm*-3*m* is 5.640 Å.[28] The primitive cell of the NaCl crystal was used, and the optimized parameter is 3.999 Å,[28] and an 8 × 8 × 8 k-point mesh was used for the relaxation. The lattice parameters (9.808 × 9.808 × 2.866 $Å^3$) of the Na_1/HMO crystal with the tetragonal space group *I*4/*m* were used according to the experimental data (Tables S1 and S2). The (001) surface of Na_1/HMO was cut based on the super cell with 36 included formula units, and an 3 × 3 × 1 k-point mesh was used for the static self-consistent calculations. The density of states (DOS) of the NaCl primitive cell and the (001) surface of Na_1/HMO were calculated.

DOI: 10.1021/acs.est.7b00499
Environ. Sci. Technol. 2017, 51, 7084–7090

RESULTS AND DISCUSSION

Structures of Single-Atom Catalysts. The tunnel openings on the (001) surfaces of HMO proved to be the catalytically active sites in the HCHO oxidation, because their size (0.26 nm[29]) was close to the thermodynamic diameter of HCHO molecule (0.24 nm[5]). Hence, depending on the types, electronic states, and precise positions, atoms anchored on the tunnel openings have an important influence on the catalytic reactivity of HMO. Silver atoms anchored on the HMO tunnel openings prepared by different methods have different electronic states, and thus they had different catalytic efficiency in HCHO oxidation.[11] The greater depletion of the *d* electronic state of Ag atoms results in stronger electronic metal−support interactions, which leads to higher catalytic activity.[11] The radius of Na^+ (~0.10 nm) is similar to that of Ag^+ (~0.10 nm).[30] Thus, sodium ions often situate at the same position of the HMO tunnel opening, more likely the crystallographic (0,0,0) sites or the Wyckoff 2*a* sites.

To identify the precise positions of Na and Ag on the tunnel openings, SXRD patterns of Ag_1/HMO and Na_1/HMO were collected and Rietveld refinement analyses were conducted (Figure 1). The structural models (insets in Figure 1) were

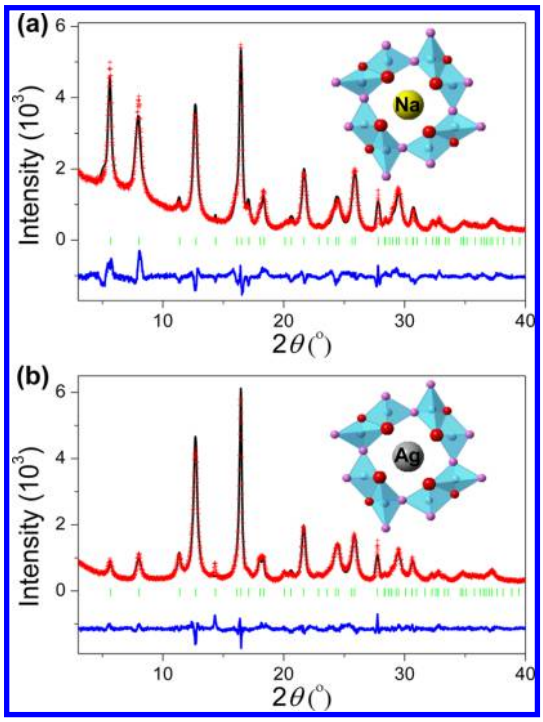

Figure 1. SXRD patterns and Rietveld refinement analyses of (a) Na_1/HMO and (b) Ag_1/HMO. The blue curves are the differential SXRD patterns. The short vertical lines below the SXRD patterns mark the peak positions of all of the possible Bragg reflections. Insets: Models showing sodium and silver atoms at the Wyckoff 2*a* sites.

constructed according to the corresponding lattice parameters and partial atom coordinates listed in Tables S1 and S2, respectively. A HMO model constructed from the SXRD pattern and refinement (Figure S1 and Tables S1 and S2) shows that HMO has one-dimensional square tunnels of ~4.7 × 4.7 $Å^2$, and a narrow position of the tunnel is located at the (002) plane,[23] which consists of 4 oxygen atoms (red balls in Figure S1) to form a square cavity. This square cavity is suitable for anchoring metal atoms such as sodium and silver at the center of the square, i.e., the position is the Wyckoff 2*a* sites. According to the refinement results (Table S2), both sodium and silver ions are situated at the same positions in the HMO tunnels. Thus, it is convenient to compare the catalytic activity of the single Na active centers with the single Ag active centers.

To investigate the influence of the incorporation of sodium or silver on the morphologies of HMO, we obtained the TEM and HRTEM images of HMO, Na_1/HMO, and Ag_1/HMO. In Figure S2, HMO grows along the tunnel direction or the [001] axis to form a rod structure, indicating that the surface energy of the (001) top-facets is much higher than that of the (100) side-facets.[31−33] Thus, the tunnel openings on the (001) top-facets often serve as catalytically active sites for the removal of some VOCs.[11,31,32] After loading sodium or silver, the rod-shaped morphology of HMO remains unchanged, and the (001) top-facets for both samples are exposed (Figure 2). Two

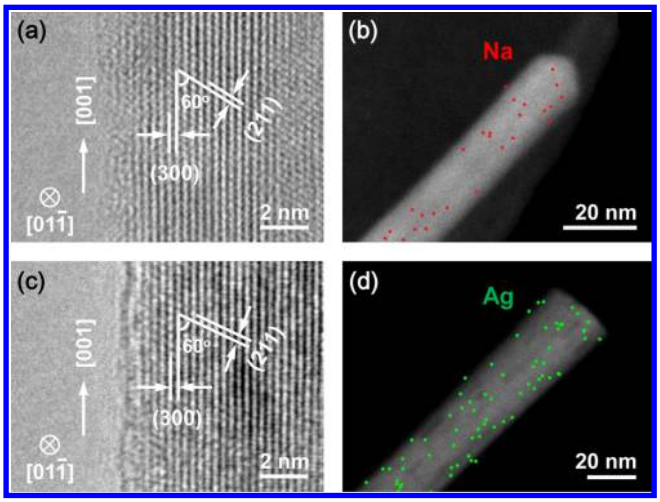

Figure 2. HRTEM (a,c), and STEM images and EDX mappings (b,d) of Na_1/HMO (a,b) and Ag_1/HMO (c,d).

fringes with a cross angle of 60° can be assigned to the (300) and (211) planes of both Na_1/HMO (Figure 2a) and Ag_1/HMO (Figure 2c), as confirmed by the corresponding fringe distances of 3.3 and 2.4 Å. Na_1/HMO and Ag_1/HMO can be more accurately written as $Na_{1.5}Mn_8O_{16}$ and $Ag_{1.2}Mn_8O_{16}$, respectively, according to the XRF analyses, which indicates that the molar fraction of Na is similar to that of Ag in HMO. The high dispersion of Na or Ag species is confirmed by EDX mapping (Figure 2b,d), and the distribution of Na or Ag on the ends of the rods is also detected, in line with the fact that the high active tunnel openings of the (001) top-facets are very suitable for anchoring metal ions such as alkalis and Ag.[11,22]

The immediate structures of anchored Ag atoms were investigated using extended X-ray absorption fine structure (EXAFS) spectroscopy. Ag *K*-edge Fourier transform (FT) EXAFS spectra of the samples are shown in Figures S3, and Figure S4 gives the curve-fitting of *R*-space and inverse FT spectra. The related structural parameters obtained by fitting the spectra with theoretical models are listed in Table S3.[34] The first amplitude of the EXAFS spectrum of Ag_1/HMO is assigned to the Ag−O bonds with an average bond length of ~2.33 Å and a coordination number of 4. The results are in line with the refinement of the corresponding XRD pattern, demonstrating that Ag atoms are at the Wyckoff 2*a* sites. Likewise, the data also agree fairly well with the fact that Ag atoms are stably fixed on the (002) plane to form planar AgO_4

DOI: 10.1021/acs.est.7b00499
Environ. Sci. Technol. 2017, 51, 7084−7090

structural motifs.[31−34] Because the Na *K*-edge EXAFS spectrum appears at significantly low absorption energies, the immediate environment of the anchored Na on the HMO planes is not obtained from its EXAFS spectrum. However, previous work with experimental and theoretical results demonstrated that sodium ions are energetically favorable to locate at a "bottleneck" on the (002) plane to form NaO_4 structural motifs, similar to the AgO_4 motifs.[29,35] As a consequence, the sodium and silver atoms are located at almost the same vacant sites on the (002) facets.

Catalytic Oxidation of HCHO. Two single-atom catalysts together with HMO were used to catalyze HCHO oxidation, because HCHO is a typical pollutant in indoor air,[1] and it can also contribute to atmospheric particulate emissions in severe haze events.[2] Our previous work reported that the tunnel openings of HMO function as catalytically active sites in the complete oxidation of HCHO.[5] Owing to the suitable size of the tunnel opening similar to the diameter of the HCHO molecule, HMO often gives better catalytic performance than β-MnO_2 and todorokite manganese oxides under identical conditions.[5]

As shown in Figure 3a, at a high GHSV of 92 000 h^{-1}, the X_{HCHO} over HMO is ~20% at 110 °C. The X_{HCHO} increases

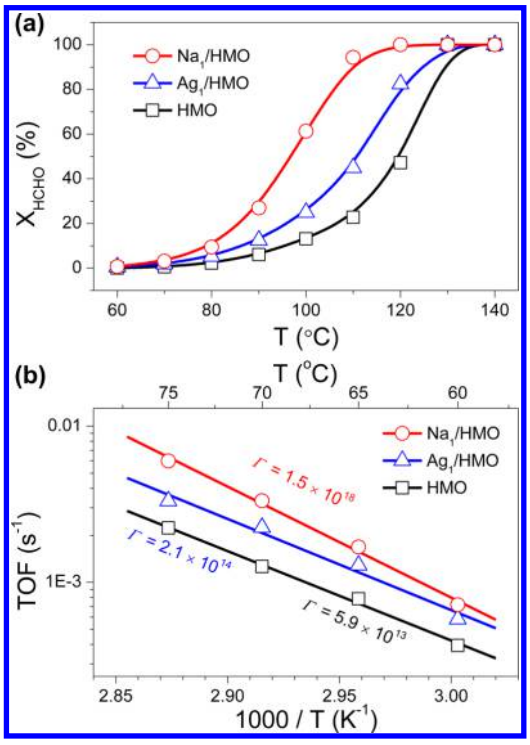

Figure 3. (a) X_{HCHO} as a function of reaction temperature (T) and (b) Arrhenius plots of HCHO oxidation over HMO, Na_1/HMO, and Ag_1/HMO.

drastically with further increasing reaction temperature, and complete oxidation of HCHO is achieved at 140 °C. Similar results were reported in the related work.[11,32] After anchoring the Na or Ag atom at the tunnel openings of HMO, the catalytic activity distinctly increases. Especially, Na_1/HMO shows much higher catalytic activity than Ag_1/HMO. The temperature required for 20% X_{HCHO} decreases to 90 °C, and 100% X_{HCHO} is achieved at 110 °C over Na_1/HMO, while complete conversion of HCHO for Ag_1/HMO occurs at 130 °C. Likewise, we recently found that single potassium ions anchored on the tunnel openings of HMO showed the same catalytic performance as Na_1/HMO.[22] The data thus indicate that single alkali atoms can be more active than single silver atoms in catalytic oxidation of HCHO.

It has been proven that the tunnel openings of HMO serve as the catalytically active centers in HCHO oxidation.[11] Three samples should have the same number of catalytically active centers per unit manganese in mole, because the exposed sodium and silver atoms are anchored on the tunnel openings of the HMO rods. Thus, we plot an Arrhenius profile, and give the pre-exponential factors (Γ) of the reaction to estimate the number of possible active centers. Although the number of sodium atoms in Na_1/HMO is almost the same as that of Ag atoms in Ag_1/HMO, and it is also similar to the number of the tunnel openings of HMO, the Γ values of Na_1/HMO (~1.5×10^{18}) and Ag_1/HMO (~2.1×10^{14}) are much larger than that of HMO (~5.9×10^{13}), implying that the accurate active centers for Na_1/HMO and Ag_1/HMO should include the surface active oxygen ions in contact with or in the periphery of sodium or silver atoms.[11] The catalytic performance of these catalysts is intimately associated with the surface lattice oxygen ions (O_s) at the periphery of sodium and silver atoms, and these O_s with nucleophilic properties are favorable to attack HCHO with the electrophilic carbonyl group.[11,16] According to our recent report,[11] ~2.7% O_s with respect to total lattice oxygen atoms are active for HCHO oxidation. Luo et al. reported similar findings that 3% O_s of HMO are responsible for complete oxidation of organic compounds.[36] Moreover, the electronic states of O_s also play an important role in determining catalytic performance.[11,36] As a consequence, two crucial factors governing the catalytic activity are the number and the electronic states of O_s. As shown in Figure 3, Na_1/HMO has the best catalytic performance and the largest Γ, possibly indicating that Na_1/HMO has more O_s available for the HCHO oxidation than the other two samples.

Activity-Structure Correlations. We further studied the electronic properties of lattice oxygen, manganese, and sodium and silver atoms, to correlate the structures with catalytic performance. O 1*s* XPS were collected to investigate the electronic density of O_s (Figure 4a). An intensive peak at a low BE of ~528 eV with a shoulder at a relatively high BE of ~531 eV is observed for three samples. The low BE peak should be ascribed to the O_s that is nucleophilic.[16] A differential XPS of Na_1/HMO by subtracting the XPS of Ag_1/HMO appears with a negative peak in the high BE regime and a positive peak in the low BE regime, evidencing that the electronic density of O_s of Na_1/HMO is higher than that of Ag_1/HMO. Thus, it has stronger nucleophilic properties, which leads to an easier reaction with electrophilic carbonyl group and further facilitates HCHO oxidation.

Furthermore, Zhang et al. has found that the O 2*p* orbitals play an important role in determining the catalytic oxidation.[37] Soft X-ray absorption spectra at the O *K*-edge were used to differentiate the electronic structures of O between Na_1/HMO and Ag_1/HMO, reflecting the interactions between O and sodium or silver.[38,39] Figure 4b shows the normalized soft X-ray absorption spectra of Na_1/HMO, Ag_1/HMO, and HMO. Three spectra exhibit two main peaks centered at ~527 and ~529 eV, which can be attributed to the transition from the O 1*s* orbitals into the t_{2g} and e_g orbitals,[39] respectively. The high energy peak intensity of Na_1/HMO with the e_g feature is slightly weak with respect to that of HMO, indicating that the occupied states of the O 2*p* orbitals with the e_g feature of Na_1/HMO increase. On

DOI: 10.1021/acs.est.7b00499
Environ. Sci. Technol. 2017, 51, 7084−7090

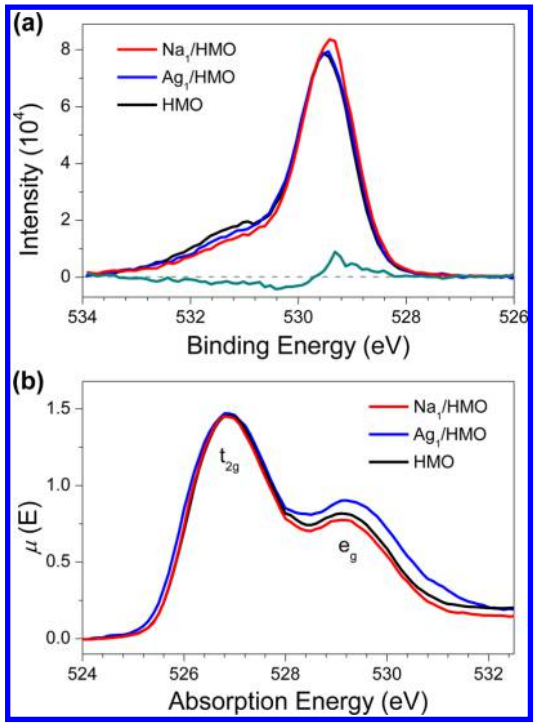

Figure 4. (a) O 1*s* XPS of Na_1/HMO, Ag_1/HMO, and HMO together with the differential XPS of Na_1/HMO with respect to that of Ag_1/HMO. (b) O *K*-edge soft-X-ray absorption spectra of Na_1/HMO, Ag_1/HMO, and HMO.

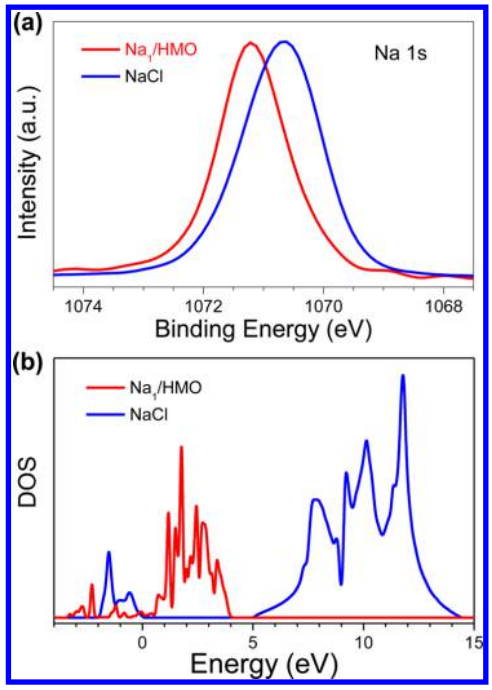

Figure 5. (a) Na 1*s* XPS of Na_1/HMO and NaCl. (b) The DOS of the Na *sp* orbitals in Na_1/HMO and NaCl.

the contrary, the O 2*p* orbitals with the e_g feature of Ag_1/HMO have the electronic density lower than those of HMO, as judged by the fact that the intensity of Ag_1/HMO at the high energy is much stronger than that of HMO. Hence, the O_s of Na_1/HMO has the O 2*p* orbitals with the high electronic density, which should be an important factor to determine the catalytic performance in the complete oxidation of HCHO.

To clarify the reasons why O_s of Na_1/HMO have higher density than those of Ag_1/HMO, the electronic properties of Na or Ag and Mn were investigated. The electronic states of Mn in three samples in terms of the average oxidation state (AOS) of Mn were estimated by Mn 2*p* and Mn 3*s* XPS data. As shown in Figure S5, the Mn $2p_{3/2}$ and Mn $2p_{1/2}$ peaks are centered at ~641.9 and ~653.6 eV, respectively, with an energy span of ~11.7 eV, implying that the Mn species are predominately Mn^{4+} for three samples.[40] To more accurately determine the AOS of Mn, the Mn 3*s* XPS are also shown in Figure S6. According to an energy difference (ΔE_{3s}) between the main peak and its satellite of the Mn 3*s* XPS, and a relationship between the ΔE_{3s} and the AOS of Mn,[41] the same AOS of Mn for all cases can be calculated to be ~3.8. In our previous studies,[11,31,32] the Ag atoms in Ag_1/HMO lose part of electrons and remain at the metallic states ($Ag^{\delta+}$, $0 < \delta < 1$). The electronic states of Na were determined by Na 1*s* XPS spectra (Figure 5a). The BE of the Na 1*s* peak shifts upward by ~0.6 eV for Na_1/HMO with respect to that of NaCl, i.e., from 1070.6 eV for NaCl to 1071.2 eV for Na_1/HMO. This indicates that the isolated sodium atoms in Na_1/HMO have lower electronic density than those in NaCl. These results indicate that the different electronic states of the surface lattice oxygen predominantly originate from the interactions of O with Na or Ag.

Generally, HCHO oxidation on metal-supported transition metal oxides follows the metal-assisted Mars-van Krevelen mechanism,[42] in which a two-stage redox process takes place: (1) the dissociation of molecular oxygen (O_2) to form O_s, and (2) the oxidation of HCHO or adsorbed formate (the stable intermediate in the HCHO oxidation reaction) by O_s:

$$O_2 + 2() \rightarrow 2(O_s) \quad (1)$$

$$HCHO + (O_s) \rightarrow (HCOOH) \quad (2)$$

$$(HCOOH) + (O_s) \rightarrow (CO_2) + (H_2O) \quad (3)$$

where () represents an active site. Therefore, the mobility and reducibility of the O_s are of crucial importance. The above results indicate that the O_s of Na_1/HMO has higher electronic density, especially in the O 2*p* orbitals, indicating that the reducibility of the O_s is improved, which will enhance the catalytic activity. Furthermore, it has been proven that the higher electronic density of the O_s of Na_1/HMO originates from Na, not from Mn, showing a strong interaction between Na and O. The DOS of Na *sp* orbitals were calculated as shown in Figure 5b. After the Na was anchored on the HMO(001) surfaces, the band gap between the lowest unoccupied molecular orbitals (LUMO) and the highest occupied molecular orbitals (HOMO) narrowed, suggesting that the electron transfer between Na and O is expected to become relatively easy.[43] Moreover, the DOS at HOMO of Na_1/HMO is relatively lower than that of NaCl, indicating that the electron transfer from Na to O occurred. This is consistent with the XPS results in Figure 5a. Therefore, sodium on the tunnel openings of HMO reduces the band gap between LUMO and HUMO and increases the reducibility of the O_s, thus being favorable for HCHO oxidation.

In conclusion, single-atom sodium and silver catalysts were synthesized by anchoring single sodium or silver atoms on the (001) surfaces of HMO, as evidenced by SXRD patterns with a structural refinement and TEM images with EDX mapping.

DOI: 10.1021/acs.est.7b00499
Environ. Sci. Technol. 2017, 51, 7084−7090

Na_1/HMO exhibited higher catalytic activity in the complete oxidation of HCHO than Ag_1/HMO. The results demonstrated that the catalytically active centers include the surface single sodium or silver and the vicinal lattice oxygen atoms, and that the electronic states of the surface lattice oxygen play a critical role in determining the catalytic performance in HCHO oxidation. The surface lattice oxygen species of Na_1/HMO with more negative charge had stronger nucleophilic properties, thus the higher efficiency than Ag_1/HMO for the abatement of HCHO. This work may provide some new insights into the design and fabrication of cheap and advanced catalysts with alkali active sites for air purification.

■ ASSOCIATED CONTENT

Supporting Information

The Supporting Information is available free of charge on the ACS Publications website at DOI: 10.1021/acs.est.7b00499.

Related tables and figures showing crystallographic data and parameters (PDF)

■ AUTHOR INFORMATION

Corresponding Author

*Phone: +86-21-65642997; fax: +86-21-65643597; e-mail: tangxf@fudan.edu.cn (X.T.).

ORCID

Xingfu Tang: 0000-0002-0746-1294

Author Contributions

§These authors contributed equally to this work.

Notes

The authors declare no competing financial interest.

■ ACKNOWLEDGMENTS

This work was financially supported by the NSFC (21477023) and the STCSM (14JC1400400). The SXRD and EXAFS measurements were conducted at the SSRF. The soft X-ray absorption spectra at the O *K*-edge were measured at the BSRF. We acknowledge Professor Xiao Gu from Chongqing University for useful discussions about DFT calculations.

■ REFERENCES

(1) *WHO Guidelines for Indoor Air Quality: Selected Pollutants*; World Health Organization Regional Office for Europe: Copenhagen, Denmark, 2010.

(2) Salthammer, T. Formaldehyde in the ambient atmosphere: From an indoor pollutant to an outdoor pollutant? *Angew. Chem., Int. Ed.* **2013**, *52* (12), 3320−3327.

(3) Long, B.; Tan, X.; Chang, C.; Zhao, W.; Long, Z.; Ren, D.; Zhang, W. Theoretical studies on gas-phase reactions of sulfuric acid catalyzed hydrolysis of formaldehyde and formaldehyde with sulfuric acid and $H_2SO_4\cdots H_2O$ complex. *J. Phys. Chem. A* **2013**, *117*, 5106−5116.

(4) Torres, J. Q.; Royer, S.; Bellat, J. P.; Giraudon, J. M.; Lamonier, J. F. Formaldehyde: Catalytic oxidation as a promising soft way of elimination. *ChemSusChem* **2013**, *6* (4), 578−592.

(5) Chen, T.; Dou, H.; Li, X.; Tang, X.; Li, J.; Hao, J. Tunnel structure effect of manganese oxides in complete oxidation of formaldehyde. *Microporous Mesoporous Mater.* **2009**, *122* (1−3), 270−274.

(6) Ma, C.; Wang, D.; Xue, W.; Dou, B.; Wang, H.; Hao, Z. Investigation of formaldehyde oxidation over Co_3O_4-CeO_2 and Au/Co_3O_4-CeO_2 catalysts at room temperature: Effective removal and determination of reaction mechanism. *Environ. Sci. Technol.* **2011**, *45* (8), 3628−3634.

(7) Zhang, C.; Liu, F.; Zhai, Y.; Ariga, H.; Yi, N.; Liu, Y.; Asakura, K.; Flytzani-Stephanopoulos, M.; He, H. Alkali-metal-promoted Pt/TiO_2 opens a more efficient pathway to formaldehyde oxidation at ambient temperatures. *Angew. Chem., Int. Ed.* **2012**, *51* (38), 9628−9632.

(8) Zhang, C.; Li, Y.; Wang, Y.; He, H. Sodium-promoted Pd/TiO_2 for catalytic oxidation of formaldehyde at ambient temperature. *Environ. Sci. Technol.* **2014**, *48* (10), 5816−5822.

(9) Yu, X.; He, J.; Wang, D.; Hu, Y.; Tian, H.; He, Z. Facile controlled synthesis of Pt/MnO_2 nanostructured catalysts and their catalytic performance for oxidative decomposition of formaldehyde. *J. Phys. Chem. C* **2012**, *116* (1), 851−860.

(10) Yu, X.; He, J.; Wang, D.; Hu, Y.; Tian, H.; Dong, T.; He, Z. Au-Pt bimetallic nanoparticles supported on nest-like MnO_2: Synthesis and application in HCHO decomposition. *J. Nanopart. Res.* **2012**, *14* (11), 1−14.

(11) Hu, P.; Amghouz, Z.; Huang, Z.; Xu, F.; Chen, Y.; Tang, X. Surface-confined atomic silver centers catalyzing formaldehyde oxidation. *Environ. Sci. Technol.* **2015**, *49* (4), 2384−2390.

(12) Chen, Y.; Huang, Z.; Zhou, M.; Hu, P.; Du, C.; Kong, L.; Chen, J.; Tang, X. The active sites of supported silver particle catalysts in formaldehyde oxidation. *Chem. Commun.* **2016**, *52*, 9996−9999.

(13) Nie, L.; Yu, J.; Li, X.; Cheng, B.; Liu, G.; Jaroniec, M. Enhanced performance of NaOH-modified Pt/TiO_2 toward room temperature selective oxidation of formaldehyde. *Environ. Sci. Technol.* **2013**, *47* (6), 2777−2783.

(14) Bai, B.; Li, J. Positive effects of K^+ ions on three-dimensional mesoporous Ag/Co_3O_4 catalyst for HCHO oxidation. *ACS Catal.* **2014**, *4* (8), 2753−2762.

(15) Zhai, Y.; Pierre, D.; Si, R.; Deng, W.; Ferrin, P.; Nilekar, A. U.; Peng, G.; Herron, J. A.; Bell, D. C.; Saltsburg, H.; Mavrikakis, M.; Flytzani-Stephanopoulos, M. Alkali-stabilized Pt-OH_x species catalyze low-temperature water-gas shift reactions. *Science* **2010**, *329*, 1633−1636.

(16) Chen, Y.; Tian, G.; Zhou, M.; Huang, Z.; Lu, C.; Hu, P.; Gao, J.; Zhang, Z.; Tang, X. Catalytic control of typical particulate matters and volatile organic compounds emissions from simulated biomass burning. *Environ. Sci. Technol.* **2016**, *50* (11), 5825−5831.

(17) Li, Q.; Wang, X.; Xin, Y.; Zhang, Z.; Zhang, Y.; Hao, C.; Meng, M.; Zheng, L.; Zheng, L. A unified intermediate and mechanism for soot combustion on potassium-supported oxides. *Sci. Rep.* **2015**, *4*, 4275.

(18) Ertl, G.; Weiss, M.; Lee, S. B. The role of potassium in the catalytic synthesis of ammonia. *Chem. Phys. Lett.* **1979**, *60* (3), 391−394.

(19) Dwyer, D. J.; Hardenbergh, J. H. Catalytic reduction of carbon monoxide over potassium modified iron surfaces. *Appl. Surf. Sci.* **1984**, *19* (1−4), 14−27.

(20) Janiak, C.; Hoffmann, R.; Sjovall, P.; Kasemo, B. The potassium promoter function in the oxidation of graphite: An experimental and theoretical study. *Langmuir* **1993**, *9* (12), 3427−3440.

(21) Xu, J.; White, T.; Li, P.; He, C.; Han, Y. Hydroxyapatite foam as a catalyst for formaldehyde combustion at room temperature. *J. Am. Chem. Soc.* **2010**, *132* (38), 13172−13173.

(22) Xu, F.; Huang, Z.; Hu, P.; Chen, Y.; Zheng, L.; Gao, J.; Tang, X. The promotion effect of isolated potassium atoms with hybridized orbitals in catalytic oxidation. *Chem. Commun.* **2015**, *51* (48), 9888−9891.

(23) Hu, P.; Schuster, M. E.; Huang, Z.; Xu, F.; Jin, S.; Chen, Y.; Hua, W.; Su, D. S.; Tang, X. The active sites of a rod-shaped hollandite deNO$_x$ catalyst. *Chem. - Eur. J.* **2015**, *21* (27), 9619−9623.

(24) Kresse, G.; Furthmuller, J. Efficient iterative schemes for *ab initio* total-energy calculations using a plane-wave basis set. *Phys. Rev. B: Condens. Matter Mater. Phys.* **1996**, *54*, 11169−11186.

(25) Kresse, G.; Furthmuller, J. Efficiency of *ab-initio* total energy calculation for metals and semiconductors using a plane-wave basis set. *Comput. Mater. Sci.* **1996**, *6*, 15−50.

(26) Perdew, J. P.; Chevary, J. A.; Vosko, S. H.; Jackson, K. A.; Pederson, M. R.; Singh, D. J.; Fiolhais, C. Applications of the

generalized gradient approximation for exchange and correlation. *Phys. Rev. B: Condens. Matter Mater. Phys.* **1992**, *46*, 6671−6687.
(27) Perdew, J. P.; Burke, K.; Ernzerhof, M. Generalized gradient approximation made simple. *Phys. Rev. Lett.* **1996**, *77*, 3865−3868.
(28) Barrett, W. T.; Wallace, W. E. Studies of NaCl-KCl solid solutions. I. Heats of formation, lattice spacings, densities, schottky defects and mutual solubilities. *J. Am. Chem. Soc.* **1954**, *76* (2), 366−369.
(29) Kijima, N.; Ikeda, T.; Oikawa, K.; Izumi, F.; Yoshimura, Y. Crystal structure of an open-tunnel oxide α-MnO_2 analyzed by Rietveld refinements and MEM-based pattern fitting. *J. Solid State Chem.* **2004**, *177* (4), 1258−1267.
(30) Shannon, R. D.; Prewitt, C. T. Effective ionic radii in oxides and fluorides. *Acta Crystallogr., Sect. B: Struct. Crystallogr. Cryst. Chem.* **1969**, *25* (5), 925−946.
(31) Huang, Z.; Gu, X.; Cao, Q.; Hu, P.; Hao, J.; Li, J.; Tang, X. Catalytically active single-atom sites fabricated from silver particles. *Angew. Chem., Int. Ed.* **2012**, *51* (17), 4198−4203.
(32) Hu, P.; Huang, Z.; Amghouz, Z.; Makkee, M.; Xu, F.; Kapteijn, F.; Dikhtiarenko, A.; Chen, Y.; Gu, X.; Tang, X. Electronic metal-support interactions in single-atom catalysts. *Angew. Chem., Int. Ed.* **2014**, *53* (13), 3418−3421.
(33) Espinal, A. E.; Zhang, L.; Chen, C. H.; Morey, A.; Nie, Y.; Espinal, L.; Wells, B. O.; Joesten, R.; Aindow, M.; Suib, S. L. Nanostructured arrays of semiconducting octahedral molecular sieves by pulsed-laser deposition. *Nat. Mater.* **2010**, *9* (1), 54−59.
(34) Chang, F. M.; Jansen, M. $Ag_{1.8}Mn_8O_{16}$: Square planar coordinated $Ag^{\oplus}$ ions in the channels of a novel hollandite variant. *Angew. Chem., Int. Ed. Engl.* **1984**, *23* (11), 906−907.
(35) Post, J. E.; Von Dreele, R. B.; Buseck, P. R. Symmetry and cation displacements in hollandites: Structure refinements of hollandite, cryptomelane and priderite. *Acta Crystallogr., Sect. B: Struct. Crystallogr. Cryst. Chem.* **1982**, *38* (4), 1056−1065.
(36) Luo, J.; Zhang, Q.; Garcia-Martinez, J.; Suib, S. L. Adsorptive and acidic properties, reversible lattice oxygen evolution, and catalytic mechanism of cryptomelane-type manganese oxides as oxidation catalysts. *J. Am. Chem. Soc.* **2008**, *130* (10), 3198−3207.
(37) Zhang, C.; Hu, P. Why must oxygen atoms be activated from hollow sites to bridge sites in catalytic CO oxidation? *J. Am. Chem. Soc.* **2000**, *122* (9), 2134−2135.
(38) Kucheyev, S. O.; van Buuren, T.; Baumann, T. F.; Satcher, J. H., Jr; Willey, T. M.; Meulenberg, R. W.; Felter, T. E.; Poco, J. F.; Gammon, S. A.; Terminello, L. J. Electronic structure of titania aerogels from soft X-ray absorption spectroscopy. *Phys. Rev. B: Condens. Matter Mater. Phys.* **2004**, *69* (24), 245102.
(39) Yoon, W. S.; Kim, K. B.; Kim, M. G.; Lee, M. K.; Shin, H. J.; Lee, J. M.; Lee, J. S.; Yo, C. H. Oxygen contribution on Li-ion intercalation-deintercalation in $LiCoO_2$ investigated by O *K*-edge and Co *L*-edge X-ray absorption spectroscopy. *J. Phys. Chem. B* **2002**, *106* (10), 2526−2532.
(40) Santos, V. P.; Carabineiro, S. A. C.; Bakker, J. J. W.; Soares, O. S. G. P.; Chen, X.; Pereira, M. F. R.; Órfão, J. J. M.; Figueiredo, J. L.; Gascon, J.; Kapteijn, F. Stabilized gold on cerium-modified cryptomelane: Highly active in low-temperature CO oxidation. *J. Catal.* **2014**, *309*, 58−65.
(41) Galakhov, V. R.; Demeter, M.; Bartkowski, S.; Neumann, M.; Ovechkina, N. A.; Kurmaev, E. Z.; Lobachevskaya, N. I.; Mukovskii, Y. M.; Mitchell, J.; Ederer, D. L. Mn 3*s* exchange splitting in mixed-valence manganites. *Phys. Rev. B: Condens. Matter Mater. Phys.* **2002**, *65* (11), 113102.
(42) Mao, C. F.; Vannice, M. A. Formaldehyde oxidation over Ag catalysts. *J. Catal.* **1995**, *154* (2), 230−244.
(43) Vayssilov, G. N.; Lykhach, Y.; Migani, A.; Staudt, T.; Petrova, G. P.; Tsud, N.; Skála, T.; Bruix, A.; Illas, F.; Prince, K. C.; Matolín, V.; Neyman, K. M.; Libuda, J. Support nanostructure boosts oxygen transfer to catalytically active platinum nanoparticles. *Nat. Mater.* **2011**, *10* (4), 310−315.

DOI: 10.1021/acs.est.7b00499
Environ. Sci. Technol. 2017, 51, 7084−7090